Journal of Naval Architecture and Marine Engineering
December, 2023
http://dx.doi.org/10.3329/jname.v20i3.70246 http://www.banglajol.info

NUMERICAL PREDICTION OF FREE SURFACE WATER WAVE FOR THE FLOW AROUND CAMBERED HYDROFOIL

Sajid Hossain[1*], Tawhidur Rahman[2], and Md. Mashud Karim[3]
[1]Naval Architecture and Marine Engineering, BUET, Dept. of NAME, BUET-1000,*sajidhossain@name.buet.ac.bd
[2]Naval Architecture and Marine Engineering, BUET, Shahid Smrity Hall, BUET-1000, tawhidurrahman98@gmail.com
[3]Naval Architecture and Marine Engineering, BUET, Dept. of NAME, BUET-1000, mmkarim@name.buet.ac.bd

Abstract:

In this study, the implicit Finite Volume Method (FVM) based on Reynolds-Averaged Navier-Stokes (RANS) equations are used to simulate the flow past a hydrofoil that is submerged in the vicinity of the free surface of water. To simulate the turbulent flow around the hydrofoil surface, realizable k-ε turbulence model is used. The Volume of Fluid (VOF) method is incorporated into the numerical simulation to capture the interface between water and air. The free surface wave generated by the stream around NACA 0012 hydrofoil is computed and compared with experimental results to validate the numerical simulation. Grid independency is checked by using three different grid sizes and the validation is done by comparing the experimental results of ratio of submergence level h/c=0.95. Finally, the cambered hydrofoil NACA 2412 is analyzed to predict the free surface water waves for seven submergence ratios, ranging from submergence level h/c= 0.95 to 5.5. The pressure coefficient, velocity contour, static pressure contour, and force coefficients are shown graphically and in tabular form for Froude number 0.57. The restricted and shallow water effects are also studied in this research. This study reveals that implicit finite volume method can predict the wave of free surface due to flow past cambered hydrofoil satisfactorily.

Keywords: Free surface water wave, finite volume method (FVM), volume of fluid (VOF), NACA 2412, hydrofoil, restricted and shallow water effect

NOMENCLATURE

c	Chord length of the hydrofoil
C_L	Lift coefficient
C_D	Drag coefficient
F_n	Froude number
g	Acceleration due to gravity
h	Height of free surface
R_e	Reynolds number
U_{avg}	Mean flow velocity
k	Turbulent kinetic energy

Greek symbols

ρ	density
α	Volume fraction
ε	Turbulent dissipation rate
μ_t	Turbulent viscosity

1. Introduction

One of the most important topics in hydrodynamics is the study of hydrofoil performance. For much marine watercraft, hydrofoils are utilized to reduce drag and improve lift force and speed. The study of the hydrofoil's hydrodynamic behavior is critical in the design of these marine boats. When the hydrofoil's submergence depth is less, the effect of free surface should be taken into account, including the profile of free surface and evaluation of forces of pressure, lift, and drag. The wave produced by a cambered hydrofoil is the subject of this research, moving in a continuous stream at a constant speed near the free surface.

The earlier works on this problem are mostly in the 2D form of hydrofoils with a free surface. At various submergence levels, angles of attack, and speeds, Duncan (1983) examined the wave elevation of free surface and breaking and non-breaking wave resistance of the NACA 0012 hydrofoil. However, the dimensions of the towing tank were adjusted in such a way that the 3D effects on the hydrofoil were diminished. Model experiments were conducted by Parkin et. al., (1956), on a symmetric Joukowski section with a thickness of 12%.

The approximation of the foil with negligible thickness with the linearized free surface condition was used both by Plotkin (1975) and Hough and Moran (1969). The flow around cambered arc hydrofoils and flat plate were studied in the first research, while the second added a correction in thickness around the leading edge.

Thick-foil approaches, such as those developed by Yeung and Bouger (1973) and Giesing and Smith (1967) gave a meticulous presentation of the flow in the vicinity of the surface of the hydrofoil. Giesing and Smith (1967) applied the kinematic body boundary condition to the Kelvin wave source on the hydrofoil surface to create an integral equation for the strength of the source, which satisfies the linearized free surface condition (Neumann condition). The integral equation was then numerically solved. Based on Green's theorem, a hybrid integral equation technique was used by Yeung and Bouger (1973). They met the requirements for an accurate body condition and linearized free surface.

For simulating free surface flow, finite volume method was used, which again, used an unstructured grid based on Euler equations that was developed by Hino (1993). Kouth et. al. (2002) investigated the behavior of a 2D hydrofoil near a free surface. Their work involved in distributing the doublet on the foil and wake surfaces and the source on an open, undisturbed surface. The linearization of free surface condition is done using the boundary condition of Dirichlet-type as opposed to the Neumann-type boundary condition.

Raza et. al. (2013) used an unsteady Reynolds Averaged Navier – Stokes code with a k –ε turbulence model and incorporated the Volume of Fluid (VOF) method to explore the effects of free surface on a hydrofoil in motion near the free surface. A grid creation during body motion was done using a dynamic mesh approach. It was found that hydrofoils have higher lift and drag coefficients and that a suction area exists that draws the submerged body up toward the free surface.

Karim et. al. (2014) evaluated the wave developed in the vicinity of the free surface that is caused by flow past a NACA 0015 hydrofoil, perpendicular to the stream. The 2D implicit Finite Volume Method (FVM) was used and the realizable k – ε turbulence model represented the turbulent flow around the hydrofoil at the free surface for solving the RANS equations. The Volume of Fluid (VOF) approach was incorporated to examine the effects of a free surface on the water. The drag and lift coefficients were investigated, as well as the hydrodynamic forces at the free surface. Ali and Karim, 2010 [11] investigated the effect of free surface on the flow around a hydrofoil that is submerged in shallow water. The standard NACA 0012 hydrofoil was used for comparison. Moreover, Uddin and Karim (2017) explored wave generation caused by the flow around a cambered hydrofoil. NACA 4412 hydrofoil section was used in this research.

Ni et al. (2021) investigated the NACA 63_4-021 hydrofoil's performance while it was moving near a free surface at various angles of attack, resulting in the determination of the lift and drag coefficient at various depths of submersion. These were determined both numerically and experimentally.

A potential flow-based panel approach was devised by Xie and Vassalos (2007) for a three-dimensional (3D) hydrofoil under a free surface. For various submergence depths, numerical results for resistance and lift coefficients, pressure and wave profiles were obtained. In order to calculate wave amplitudes, lift, and drag forces, the main focus of this study is to determine how free surface waves for submerged hydrofoils arise at different submergence depths. The interface capturing approach is used to mimic a problem in which both fluids (water and air) are treated as if they were a single effective fluid. This approach is initially applied to the NACA 0012 hydrofoil in order to compare the findings to Duncan's experimental results. The approach is therefore applied to the NACA 2412 hydrofoil at Froude number 0.5711 and Reynold's number 1.592×10^5 to get wave altitudes, the colored contour of the magnitude of the static pressure and velocity near the hydrofoil, and the values of drag and lift coefficients for various submergence depths. The whole simulation is conducted under three-dimensional coordinates of hydrofoil and domain.

2. Mathematical Background

Results from the CFD (Computational Fluid Dynamics) are acquired by applying the finite volume approach to solve RANS equations. The governing equations, continuity and momentum equations are as follows:

- Continuity equation:

$$\frac{\partial u_j}{\partial x_i} = 0 \tag{1}$$

- Equation of momentum:

$$\frac{\partial}{\partial x_j}\left(\rho u_i u_j\right) = -\frac{\partial P}{\partial x_j} - \frac{\partial}{\partial x_j}\left(\tau_{ij} + \rho\overline{u_i' u_j'}\right) \tag{2}$$

Reynolds Averaged Navier-Stokes (RANS) equation is used to describe the incompressible viscous flow field around a submerged hydrofoil. Reynolds stress $-\rho\overline{u_i' u_j'}$ must be properly described for this RANS equation. Below is a description of the governing equation of the flow field and the mathematical formulation of the turbulence model.

In Cartesian tensor notation, the RANS equations are written as:

$$\frac{\partial \rho}{\partial t} + \frac{\partial}{\partial x_j}\left(\rho u_i\right) = 0 \tag{3}$$

and

$$\frac{\partial(\rho u_i)}{\partial t} + \frac{\partial\left(\rho u_i u_j\right)}{\partial x_j} =$$

$$-\frac{\partial p}{\partial x_i} + \frac{\partial}{\partial x_j}\left(\mu\left(\frac{\partial u_i}{\partial x_j} + \frac{\partial u_j}{\partial x_i}\right) - \frac{2}{3}\delta_{ij}\frac{\partial u_i}{\partial x_j}\right) + \frac{\partial}{\partial x_j}\left(-\rho\overline{u_i' u_j'}\right) \tag{4}$$

The Reynolds stresses and mean velocity gradients can be related using the Boussinesq hypothesis as shown below.

$$-\rho\overline{u_i' u_j'} = \mu_t\left(\frac{\partial u_i}{\partial x_j} + \frac{\partial u_j}{\partial x_i}\right) - \frac{2}{3}\left(\rho k + \mu_t\frac{\partial u_k}{\partial x_k}\right)\delta_{ij} \tag{5}$$

The realizable k-ε turbulence model equations are given by:

$$\frac{\partial}{\partial t}\left(\rho k\right) + \frac{\partial}{\partial x_j}\left(\rho k \mu_j\right) = \frac{\partial}{\partial x_j}\left[\left(\mu + \frac{\mu_t}{\sigma_k}\right)\frac{\partial k}{\partial x_j}\right] +$$

$$G_k + G_b - \rho\varepsilon - Y_M + S_k \tag{6}$$

and

$$\frac{\partial}{\partial t}\left(\rho\varepsilon\right) + \frac{\partial}{\partial x_j}\left(\rho\varepsilon\mu_j\right) = \frac{\partial}{\partial x_j}\left[\left(\mu + \frac{\mu_t}{\sigma_\varepsilon}\right)\frac{\partial \varepsilon}{\partial x_j}\right]$$

$$+\rho C_1 S_\varepsilon + \rho C_2\frac{\varepsilon^2}{k + \sqrt{\nu\varepsilon}} + C_{1\varepsilon}\frac{\varepsilon}{k}(C_{3\varepsilon}G_b) + S_\varepsilon \tag{7}$$

Where,

$$C_1 = \max\left[0.43, \frac{\eta}{\eta + 5}\right],\ \eta = S\frac{k}{\varepsilon}$$

These equations have C_2 and C_1 as constants, σ_k and σ_ε as the turbulent Prandtl numbers for and, respectively, and S_k and S_ε as user-defined source terms. G_k represents the generation of turbulent kinetic energy due to mean velocity gradients, while G_b represents the generation of turbulent kinetic energy due to buoyancy. Y_M represents the contribution of the fluctuating dilatation incompressible turbulence to the overall dissipation rate. The turbulent viscosity μ_t is computed by combining k and ε as follows:

$$\mu_t = \rho C_\mu\frac{k^2}{\varepsilon} \tag{8}$$

where C_μ is a constant.

The turbulent kinetic energy is given by,

$$k = \frac{3}{2}\left(U_{avg} I\right)^2 \tag{9}$$

Where U_{avg} is the mean flow velocity and I is the turbulence intensity=$0.16(Re)^{-1/8}$ and the turbulence dissipation rate ε is given by,

$$\varepsilon = C_{\mu}^{3/4} \frac{k^{-3/2}}{l} \tag{10}$$

where, l=0.07L

To simulate the free surface wave generation, VOF method is used. The governing equation of this method is given by:

$\frac{DF}{Dt} = \frac{\partial F(\vec{x},t)}{\partial t} + (\vec{V}\nabla)F(\vec{x},t) = 0$

Where F is defined as a function whose value is unity when the space is occupied as fluid. The value of F is 1 when a cell is full of fluid and the value is 0 when a cell is totally void of fluid. So, a value between zero and one contains a free surface.

3. Numerical Simulation

NACA 0012 and NACA 2412 2D (XY) coordinates are taken from Abbott and Doenhoff (1959) and imported into STAR-CCM+ software. For NACA 0012 hydrofoil, it is extruded to 0.1m and NACA 2412 is extruded to both 0.1m and 0.2m along the Z direction (see Figure 1).

Figure 1: 3D model of NACA 0012 hydrofoil (Left) and NACA 2412 hydrofoil (Right)

Figure 2 depicts the computational domains in the XY plane for two conditions. The first domain has a length of 15C (3.045m) and a breadth of 10C (2.03m). The left and right sides of the domain are inlet and outlet respectively and the top and bottom are taken as walls.

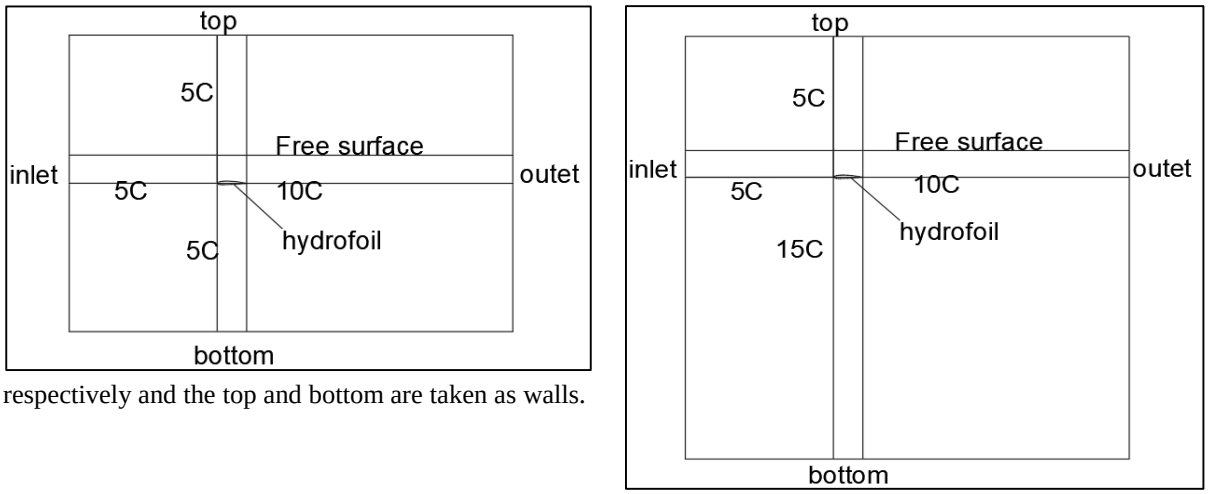

Figure 2: Computational Domain 1 & 2 (XY Plane)

The hydrofoil is located 5C (1.015m) from the inlet and 5C (1.015m) from the top wall. The line of the free surface is initially constructed at 0.95C (0.1929m) above the hydrofoil. On the other hand, the second domain has the only

difference from the first domain in breadth, which is 15C (3.045m). The other dimensions are the same as the first one. Table 1 shows the boundary conditions. For restricted wall condition the boundary of both sides are set as wall instead of symmetry plane.

Table 1: Boundary Conditions

Boundaries	**Boundary Conditions**
Inlet	Velocity Inlet
Outlet	Pressure Outlet
Top	Velocity Outlet
Bottom	Wall
Left Side	Symmetry Plane
Right Side	Symmetry Plane

The surface remesher is used for surface mesh and for volume mesh trimmer meshing model is used. The prism layer mesher is used to mesh around the hydrofoil wall. Volumetric controls are used at different locations to refine the mesh as shown in Figure 3.

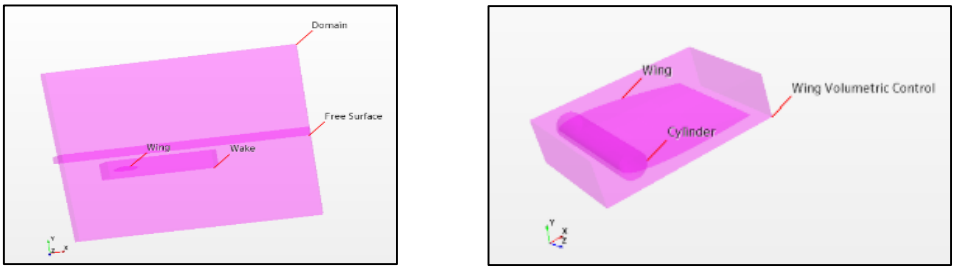

Figure 3: Volumetric control for free surface and wake refinement (Left) and for leading and hydrofoil (Right**)**

To solve the Reynolds Averaged Navier-Stokes (RANS) equation implicit finite volume method is used. To capture the turbulent flow the realizable k-ε is used. Volume of fluid method is used to find out the free surface effect. The implicit unsteady is used as a time model.

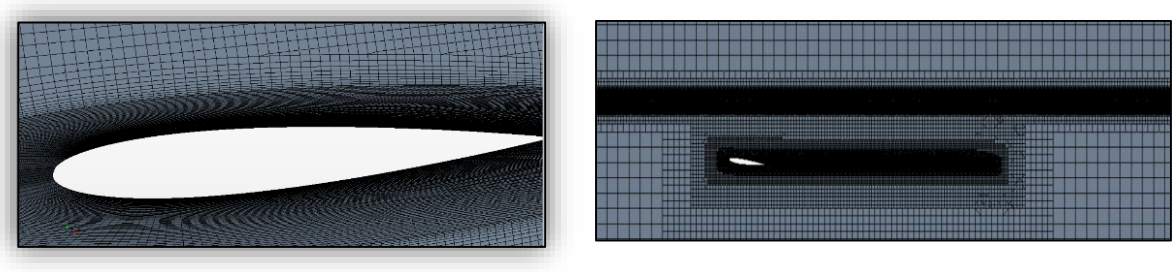

Figure 4: Mesh scene (Left) and Prism layer (Right)

4. Results & Discussion

By maintaining the identical conditions as the experiment carried out by Duncan (1983), the simulation of the NACA 0012 hydrofoil is carried out in order to validate the numerical results. A hydrofoil with chord length 20.3cm, speed 0.8ms^{-1}, Froude number 0.57, Reynolds number 1.59 x 10^5, and angle of attack 5^o is modeled to compare the numerical results with the experiment conducted by Duncan (Figure 5).

In Figure 6, free surface of NACA 0012 and NACA 2412 are compared. The crests coincide but the trough of NACA 2412 is greater. Lift and drag coefficient of NACA 2412 is higher than NACA 0012 in presence of free surface which means resistance increases in NACA 2412. The C_L and C_D values are given in Table 2.

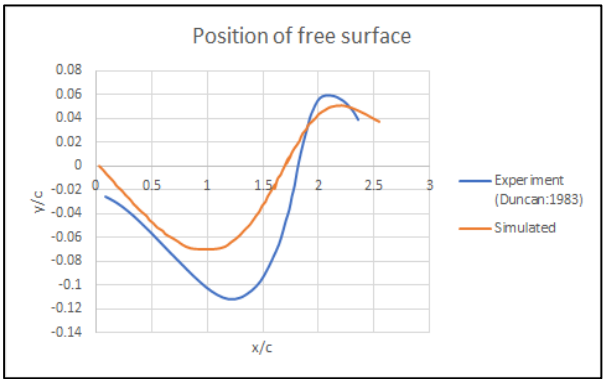

Figure 5: Comparison of simulated and experimental results

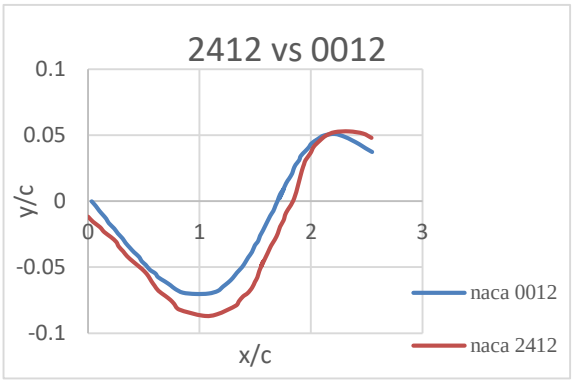

Figure 6: Free surface comparison between NACA 0012 and NACA 2412

Table 2: Force coefficients for symmetric foil vs cambered foil

	NACA 0012	NACA 2412
C_L	0.526	0.610
C_D	0.024	0.024

To determine the grid convergence of the results, three grids are used. The force coefficients of NACA 2412 tend to converge when 3502920 cells are used. The rest are illustrated in Table 3.

Table 3: Grid convergence test

Grid	Base Size	Cell Number	C_L	C_D
1	1 m	893474	0.620	0.026
2	0.6 m	2349944	0.610	0.025
3	0.5 m	3502920	0.610	0.024

In Figure 7, boundary effects are shown. When the left and right sides are taken as wall, the results show resemblance with towing tank experiments as the sides of the tank are wall. However, in open water condition, symmetry plane is the appropriate boundary condition. The lift coefficient is more in open water condition. This occurs due to restricted wall effect. Table 4 shows the force coefficients with boundary effects.

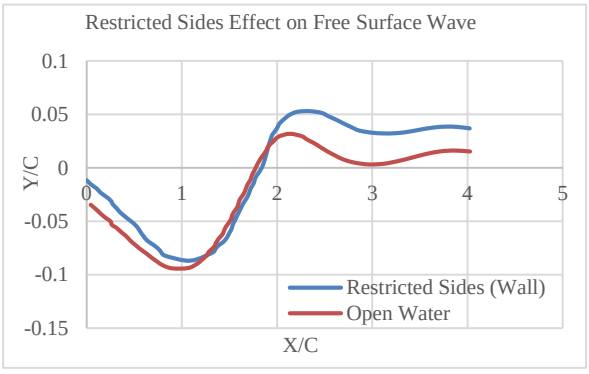

Figure 7: Free surface wave for different sides conditions

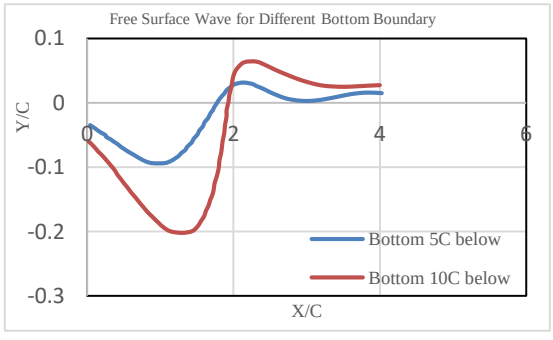

Figure 8: Free surface for different bottom conditions

Table 4: Force co-efficient for different boundary conditions at sides

	Wall	Symmetry plane
C_L	0.610	0.663
C_D	0.024	0.023

Figure 8 shows the free surface position as the depth of the domain is varied. When the bottom boundary is taken to be 10C the wave crest and trough become larger than 5C. Therefore, in shallow water conditions, the wave elevation has lower values. The lift coefficient is also less in shallow water conditions. Table 5 shows the force coefficients for different bottom conditions.

Table 5: Force coefficient for different bottom conditions

	C_L	C_D
Bottom below 5C	0.663	0.023
Bottom below 10C	0.848	0.054

The comparison between current computational results and experimental ones by Duncan is shown in Figure 5. The simulated elevations of the wave correlate well with wave elevations determined experimentally, as seen in the figure. The NACA 2412 hydrofoil section is then numerically simulated under the identical circumstances as previously indicated for various submergence depths.

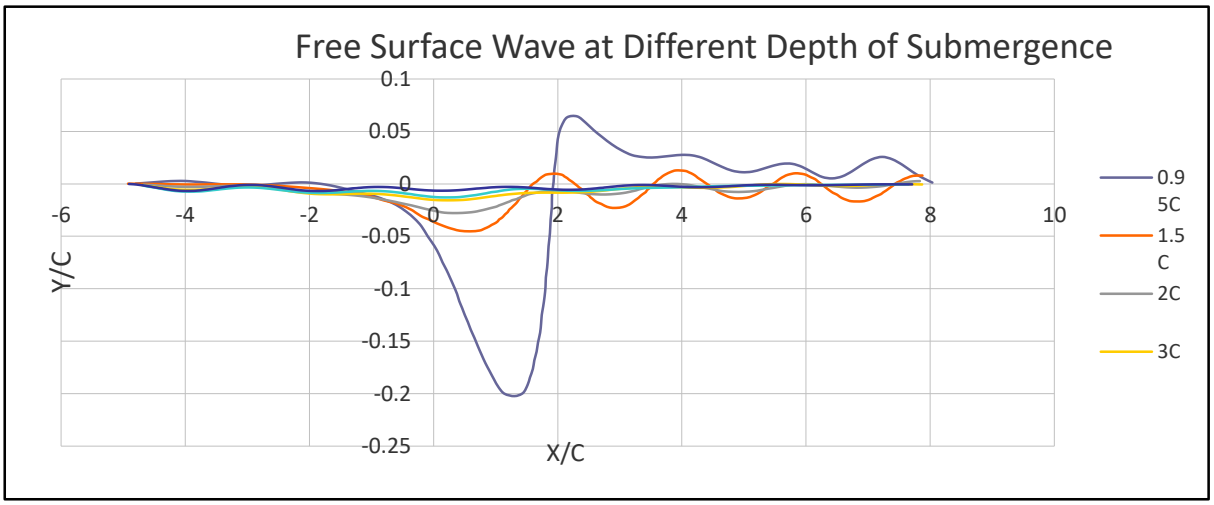

Figure 9: Comparison of wave elevation for NACA 2412 hydrofoil at different h/c ratios

The wave elevation for distinct submergence ratio h/c are shown in Figure 9. The maximum values of the crest and trough gradually decrease as the submergence level increases and the waves tend to damp away as the waves progress, which shows that the waves will damp out as the waves progress further. Moreover, the figure shows that effect on hydrofoil from h/c = 4 is negligible, that is, there is no wave elevation from this particular submergence level. C_L and C_D do not vary.

Figure 10 delineated the velocity contour at submergence level 1.5C where the fluid velocity is greater beneath the trough and above the crest and smaller than the average value above the trough and under the crest.

For each curve in Figure 11, the upper curve illustrates the pressure coefficient distribution around the lower surface of the hydrofoil and the lower curve is for upper surface. For submergence level 0.95C it is seen that the Cp for upper surface is about -3 on the leading edge. As the submergence level increases the magnitude of Cp decreases. However, on the lower surface, the pressure coefficient distribution is 1 for submergence depth 0.95C and barely changes with submergence level. So, it can be said that there is a substantial effect of free surface on the upper surface but the effect on the lower surface of the hydrofoil is negligible.

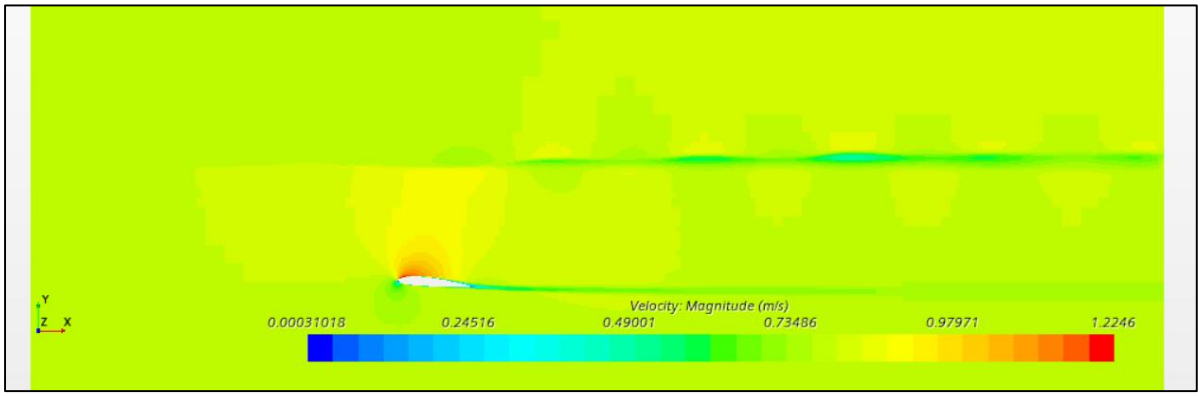

Figure 10: Contour of velocity magnitude around NACA 2412 at submergence level 1.5C

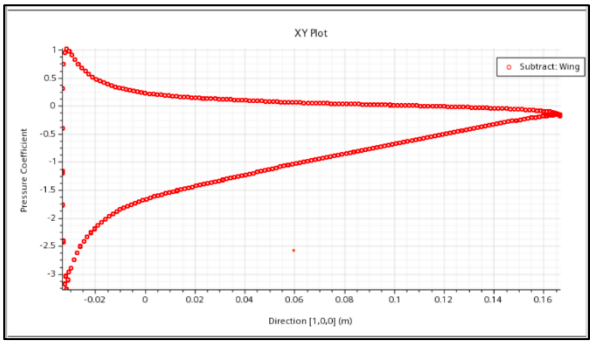

(a)

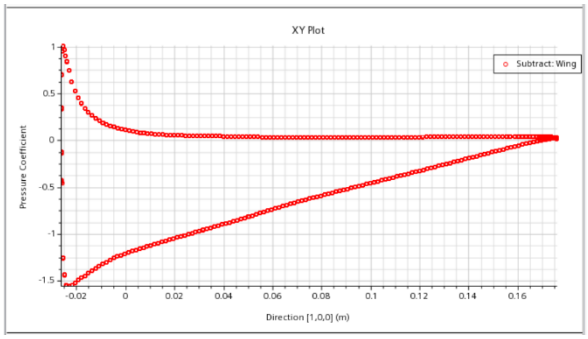

(b)

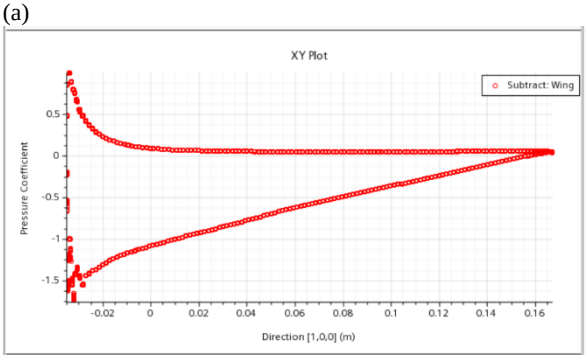

(c)

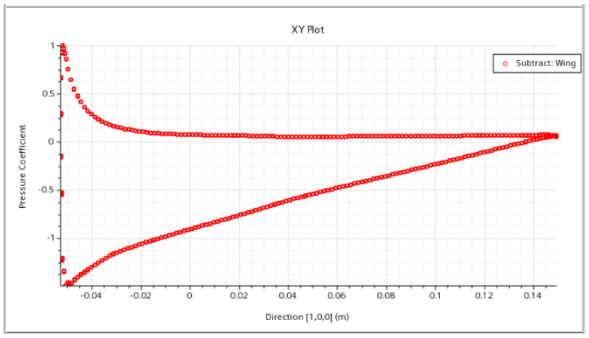

(d)

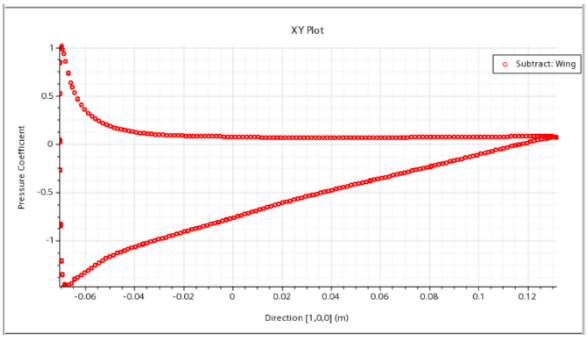

(e)

Figure 11: Pressure coefficient distribution around hydrofoil for submergence level (a) 0.95C (b) 1.5C (c) 2C (d) 3C and (e) 4C respectively

Table 6: Pressure on hydrofoil for different submergence depth

Submergence Depth	**Max. Pressure (Pa)**	**Min. Pressure (Pa)**
0.95C	319.6	-1020.6
1.5C	315.2	-496.7
2C	316.8	-526.8
3C	320	-471.7
4C	321.3	-468.2

Table 7: Force coefficients at $\alpha = 5^o$ and Fn = 0.57 (C is chord length

Submergence depth	Lift Coefficient	Drag Coefficient
0.95C	0.848	0.054
1.5C	0.634	0.013
2C	0.621	0.012
3C	0.612	0.012
4C	0.61	0.012
4.5C	0.61	0.012
5.5C	0.61	0.012

Table 6 summarizes the maximum and minimum pressure on the surface of hydrofoil for each submergence level. Table 7 shows the lift and drag coefficients for various submergence levels of NACA 2412 hydrofoil at 5^o angle of attack. Although the lift and drag coefficients increase as the depth increases for higher Froude number however, if Froude number is taken less, the force coefficients decrease as submergence level increases (Xie and Vassalos, 2007). Since, in this research project the Froude number is low, the results match with the latter phenomenon.

5. Conclusion

The production of free surface water wave for the flow around a cambered hydrofoil at various submergence ratios is calculated using the implicit finite volume method (FVM), which incorporates the volume of fluid method (VOF), and realizable k-ε turbulence model. These conclusions are come up with, from results and discussion:

- The implicit finite volume method can satisfactorily analyze the flow around the cambered hydrofoil with NACA 2412 section.
- The volume of the fluid approach together with the realizable *k-ε* turbulence model may satisfactorily estimate the wave created by the flow around the hydrofoil moving close to the free surface.
- The CFD method also computes hydrodynamic forces satisfactorily.
- The lift coefficient for the restricted water condition becomes less than that for the open water condition. It also decreases in the shallow water region.
- The pressure coefficient distribution varies only on the upper surface of the hydrofoil due to the free surface effect.
- The ratio of submergence depth greater than four can be taken as the deep-water case since the free surface effect is not observed while there was a flow around the hydrofoil.

References

Abbott, I.H., von Doenhoff, A.E. (1959). Theory of wing sections including a summary of wing foil data, Dover Publications.

Ali, M.A., Karim. M.M. (2010). Numerical study of free surface effect on the flow around shallowly submerged hydrofoil. Proceedings of the International Conference on Marine Technology (MARTEC 2010). Dhaka.

Duncan, J.H. (1983). The breaking and non-breaking wave resistance of a two-dimensional hydrofoil. J. Fluid Mech., 126, 507-520. https://doi.org/10.1017/S0022112083000294

Giesing, J.P., Smith, A.M.O., (1967). Potential flow about two-dimensional hydrofoils. Journal of Fluid Mechanics, 28, 113-129. https://doi.org/10.1017/S0022112067001934

Hino, T. (1993). A finite-volume method with unstructured grid for free surface flow. Sixth International Conference on Numerical Ship Hydrodynamics. Tokyo.

Hough, G.R., Moran, S.P. (1969). Froude number effects on two-dimensional hydrofoils. Journal of Ship Research,13(1), 53-60. https://doi.org/10.5957/jsr.1969.13.1.53

Karim, M.M., Prashad, B., Rahman, N. (2014). Numerical simulation of free surface water wave for the flow around NACA 0015 using the volume of fluid (VOF) method. Ocean Engineering, 78, 89-94.
https://doi.org/10.1016/j.oceaneng.2013.12.013

Kouth, J.S., Lin, T.J., Chau, S.W. (2002). Performance analysis of two-dimensional hydrofoil under free surface. J Eng Natl Taiwan Univ.

Ni, Z., Dhanak, M., Su, T. (2021). Performance of a hydrofoil operating close to a free surface over a range of angles of attack. International Journal of Naval Architecture and Ocean Engineering, 14, 317-336.
https://doi.org/10.1016/j.ijnaoe.2020.11.002

Parkin, B.R., Perry, B., Wu, T.Y. (1956). Pressure distribution of hydrofoil running near the water surface. Journal of Applied Physics, 27, 232-240. https://doi.org/10.1063/1.1722350

Plotkin, A. (1975). Thin hydrofoil thickness problem including leading edge corrections. Journal of Ship Resolutions, 19, 122-129. https://doi.org/10.5957/jsr.1975.19.2.122

Raza, N., Mehmood, I., Rafiuddin, H., Bilal, S., Rafique, M. (2013). Numerical simulation of free surface effect on moving hydrofoil near free surface. 10th International Bhurban Conference on Applied Science & Technology, (pp- 249-255). Islamabad. https://doi.org/10.1109/IBCAST.2013.6512162

Uddin, M.I., Karim, M.M. (2017). Application of Volume of Fluid (VOF) method for prediction of wave generated by flow around cambered hydrofoil. Procedia Engineering, 194. 82-89.
https://doi.org/10.1016/j.proeng.2017.08.120

Xie, N., Vassalos, D. (2007). Performance analysis of 3D hydrofoil under free surface. Ocean Engineering, 34, 1257-1264. https://doi.org/10.1016/j.oceaneng.2006.05.008

Yeung, R.W., Bouger, Y.C. (1979). A hybrid-integral equation method for steady two-dimensional ship waves. International Journal for Numerical Methods in Engineering, 14, 317-336.
https://doi.org/10.1002/nme.1620140303